THE EUROPEAN
PHYSICAL JOURNAL C

Deep-underground search for the decay of ^{180m}Ta with an ultra-low-background HPGe detector

R. Cerroni[1], S. Dell'Oro[2,3], A. Formicola[4], S. Ghislandi[1,5], L. Ioannucci[6], M. Laubenstein[1,a], B. Lehnert[7],
S. S. Nagorny[8,9], S. Nisi[1], L. Pagnanini[1,5,9]

[1] INFN-Laboratori Nazionali del Gran Sasso, 67100 Assergi, L'Aquila, Italy
[2] Università di Milano-Bicocca, 20126 Milan, Italy
[3] INFN-Sezione di Milano-Bicocca, 20126 Milan, Italy
[4] INFN-Sezione di Roma, 00185 Rome, Italy
[5] Gran Sasso Science Institute, 67100 L'Aquila, Italy
[6] INFN-Laboratori Nazionali di Frascati, 00044 Frascati, Rome, Italy
[7] Nuclear Science Division, Lawrence Berkeley National Laboratory, Berkeley, CA 94720, USA
[8] Arthur B. McDonald Canadian Astroparticle Physics Research Institute, Kingston, ON K7L-3N6, Canada
[9] Department of Physics, Enigneering Physics and Astronomy, Queen's University, Kingston, ON K7L-3N6, Canada

Abstract ^{180m}Ta is the longest-lived metastable state presently known. Its decay has not been observed yet. In this work, we report a new result on the decay of ^{180m}Ta obtained with a 2015.12-g tantalum sample measured for 527.7 d with an ultra-low background HPGe detector in the STELLA laboratory of the Laboratori Nazionali del Gran Sasso (LNGS), in Italy. Before the measurement, the sample has been stored deep-underground for ten years, resulting in subdominant background contributions from cosmogenically activated ^{182}Ta. We observe no signal in the regions of interest and set half-life limits on the process for the two channels EC and β^-: $T_{1/2,\ \mathrm{EC}} > 1.6 \times 10^{18}$ year and $T_{1/2,\ \beta^-} > 1.1 \times 10^{18}$ year (90% C.I.), respectively. We also set the limit on the γ de-excitation / IC channel: $T_{1/2,\ \mathrm{IC}} > 4.1 \times 10^{15}$ year (90% C.I.). These are, as of now, the most stringent bounds on the decay of ^{180m}Ta worldwide. Finally, we test the hypothetical scenarios of de-excitation of ^{180m}Ta by cosmological Dark Matter and constrain new parameter space for strongly-interacting dark-matter particle with mass up to 10^5 GeV.

1 Introduction

Tantalum (Ta) has a nearly mono-isotopic composition: the natural abundances are in fact 0.9998799(32) of ^{181}Ta and 0.0001201(32) of ^{180m}Ta, while the ground state of ^{180}Ta is not present, having a half-life of 8.15 h [1]. The tiny fraction of ^{180m}Ta was first measured in 1955 [2,3], although at that time it was not understood that it belonged to an isomeric state. Since then, significant interest has been demonstrated in probing the half-life of ^{180m}Ta, given the rather unique situation in nature and the impact in astrophysics. Indeed the half-life of ^{180m}Ta directly affects its observed abundance, and hence its production mechanism, which in turn is a probe for the production of heavy elements in stellar nucleosynthesis [4–6].

The decay scheme of ^{180m}Ta is shown in Fig. 1. Two possible branches lead to ^{180}W and to ^{180}Hf via electron capture (EC) and β^- decay, respectively, while a γ de-excitation / internal conversion (IC) from the 9^- isomeric state to the 2^+ state is also possible. Recent calculations of the nuclear matrix elements for the transition give an estimate for the half-life of 1.4×10^{20} year (EC), 5.4×10^{23} year (β^-) and 8×10^{18} year (IC), dominated by the latter channel [7]. It is worth noting that the Authors of Ref. [7] hint for an overall factor 2 of uncertainty for their calculations and push for further experimental measurements.

Over the years, different techniques have been used to experimentally search for the decay of ^{180m}Ta (Fig. 2). The early limits set by mass spectrometry were soon overcome by the more powerful γ-spectrometry measurements, initially performed with scintillators and later with germanium Ge(Li) detectors; more recently, stringent results have been obtained by using High-Purity Germanium (HPGe) detectors. As of today, neither of the radioactive decays has been observed and
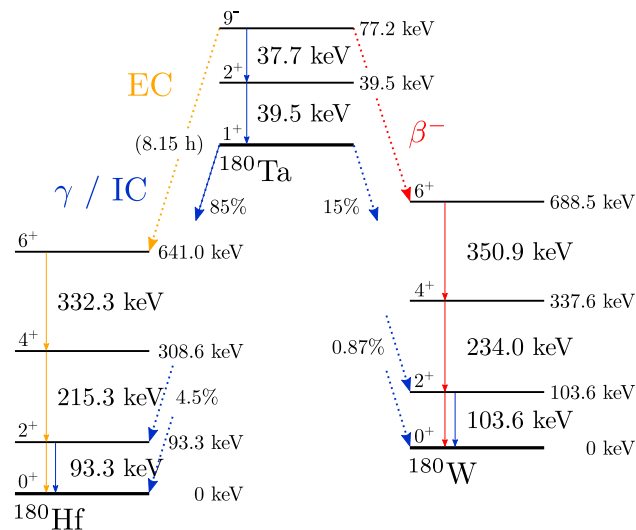
Springer

Fig. 1 Decay scheme of ^{180m}Ta [16]. The EC, β^- and γ/IC branches are shown in different colors, while the experimental signatures for γ spectroscopy are highlighted
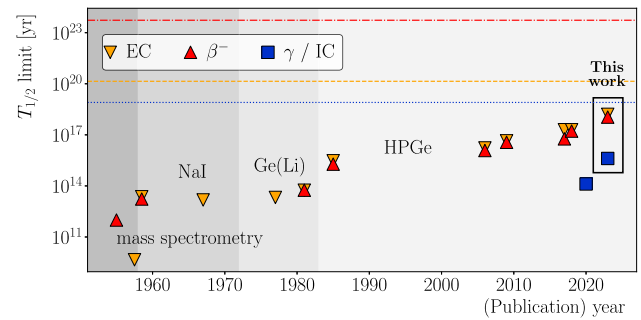

Fig. 2 Lower limits on the decay half-life of ^{180m}Ta on the EC, β^- and γ / IC channels [9,18–28]; the box encloses the new results presented in this work. The labels and corresponding shadowed areas refer to the different techniques used for the measurements. The horizontal lines indicate the theoretical half-lives from the calculations of the nuclear matrix elements [7]: EC (dashed), β^- (dash-dotted) and γ / IC (dotted)

the current overall limit on the process is $T_{1/2} > 9.03 \times 10^{16}$ year at 90% C. L. [8,9].[1]

In this work, we present new results on the search for the decay of ^{180m}Ta, where we exploit the excellent performance of the ultra-low-background HPGe (ULB-HPGe) detectors in the SubTerranean Low-Level Assay (STELLA) laboratory [10,11] at Laboratori Nazionali del Gran Sasso, in Italy. The average overburden of 3600 m w. e. and the mostly-calcareous rock composition of the Gran Sasso mountain [12] guarantee very low muon and neutron fluxes of about 3×10^{-8} cm^{-2} s^{-1} [13,14] and 4×10^{-6} cm^{-2} s^{-1} [15], as well as a relative low content of natural radioactivity in the surrounding rock. In addition to the deep-underground location, the strict protocols adopted in order to select only radio-clean materials for the detectors and shield parts result in a strong abatement of the background due to internal and environmental radioactive content.

2 Sample description and preparation

The sample was procured in 2009 and consists of 6 tiles of metallic Ta produced via vacuum melting by Advent Research Material Ltd. Each tile measures $10 \times 10 \times 0.2$ cm^3 and has a mass of ~ 335 g, corresponding to a total of about 2 kg.

In order to mitigate the intrinsic background due to cosmogenic activation of ^{182}Ta ($T_{1/2} = 114.74$ d [17]), the tiles have been stored deep-underground in the STELLA labora-

tory until the start of measurements in 2019. This corresponds to about 30 half-lives and reduced the ^{182}Ta background contribution to subdominant levels.

Before starting the measurement campaign, the Ta sample underwent a chemical treatment aimed at reducing the surface contamination. We deemed that removing the outermost 5 μm (per side) of each tile would represent a good compromise between an effective cleaning and an affordable mass loss. We tested different acid mixtures to assess the corresponding etching action. We observed that pure HF was not powerful, as it resulted in a 0.02 μm min^{-1} erosion, while adding a small amount of HNO$_3$ and H$_2$SO$_4$, easily increased the erosion speed to more than 60 μm min^{-1}.

In the end, we adopted the composition: HF(20 M) + HNO$_3$(0.35M)+H$_2$SO$_4$(1.1M). We immersed each Ta tile in 170 ml of this solution for 70 s, then rinsed it with ultra-pure water for 30 s and finally dried it with N$_2$ gas. This procedure removed between 4 and 5 μm of the surface (see Table 1). After the cleaning, the tiles were vacuum sealed into two nested plastic bags, of which the internal one remained also during the measurement (the absorption effect on γ radiation is negligible). Since the cleaning operations could only be performed in the above-ground chemistry laboratory, we had to prevent that the cosmogenic activation of ^{182}Ta could spoil the effect of the 10-year-long storing deep-underground. We thus minimized the time spent above-ground by allowing only one tile at a time to leave the STELLA laboratory and cleaning each of the 6 tiles individually. In this way, we were able to ensure that no tile spent more than 30 min outside the Gran Sasso tunnel.

After the chemical treatment described above, the total sample mass was 2015.12 g (Table 1), corresponding to 242.02 mg of ^{180m}Ta.

---

[1] This result only considers the combination of EC and β^- decay and is reported as preliminary in the cited proceedings.

Table 1 Mass of the Ta tiles before and after the cleaning treatment. The thickness reduction is estimated by assuming a uniform loss of material. The time spent outside the tunnel by each tile is also reported

Tile	m_{in} (g)	m_{fin} (g)	Δm (g)	Δx (μm)	t_{out} (min)
1	339.75	338.15	1.60	4.80	25
2	337.61	336.22	1.39	4.16	20
3	341.72	340.38	1.34	4.01	29
4	337.46	335.93	1.53	4.58	29
5	333.05	331.67	1.38	4.13	27
6	334.30	332.77	1.53	4.58	27

Fig. 3 (Left) the Ta sample consists of six tiles. (Right) the tiles arranged inside the Marinelli

3 Measurement

The measurement of the Ta sample was carried out with an ULB-HPGe detector in the STELLA laboratory [29,30]. The detector has a p-type germanium crystal with a volume of about 400 cm^3; the counting efficiency has been optimized using a Marinelli-type geometry. The energy resolution measured with a high-statistics run is (2.06 ± 0.06) keV Full Width Half Maximum (FWHM) at the 1461-keV peak of ^{40}K.

To reduce the external background, the detector is encased in a multi-layer shield consisting of (from inside to outside) 5 cm of electrolytic copper and low-radioactivity lead (30 cm from the bottom and 25 cm from the sides). The sample chamber has a volume of about 15 l ($250 \times 250 \times 240$ mm^3). The shield, together with the cryostat, is enclosed in an air-tight steel housing of 1-mm thickness, which is continuously flushed with highly-pure nitrogen gas in order to abate the radon-induced background.

Figure 3 shows the Ta-sample configuration during the measurement. The six tiles have been arranged inside a Marinelli-type beaker forming a cubic box around the detector end cap. Two tiles were placed on the top and a single tile on each lateral side.

We acquired data over a 4-year period, from January 2019 to November 2022, for a total live-time of about 1.45 year. The measurement campaign comprises 13 runs of variable duration, from a few days up to three months (Table 2). We could not operate continuously since the detectors of

Table 2 Live time and start date of the runs analyzed in this work as divided into four major datasets. The discontinuities in the data acquisition are due to the fact that the STELLA facility is primarily assigned to the radio-assay and screening of materials. During the whole 4-year period, the Ta sample always remained inside the Marinelli-type beaker in the same configuration, constantly flushed with nitrogen

Run	Start	t_{live} [d]
Dataset I		
1	Jan 2019	43.0
2	Jun 2019	41.5
3	Aug 2019	59.3
Dataset II		
4	Feb 2020	58.9
5	Apr 2020	40.4
Dataset III		
6	May 2021	61.3
7	Jul 2021	5.9
8	Jul 2021	100.6
Dataset IV		
9	Mar 2022	46.8
10	Jul 2022	29.7
11	Sep 2022	5.9
12	Sep 2022	11.7
13	Oct 2022	22.5

the STELLA laboratory are mainly devoted to radio-assay and screening of the materials to be employed in rare-event search experiments. For this reason we combined the collected runs into 4 datasets interspersed by the stop periods. All data have been acquired in the same sample-detector configuration and no significant difference between the datasets has been observed.

4 Data analysis

As a first step, we calibrated each dataset by referring to a set of background peaks from internal contamination of either the detector or the sample, namely ^{214}Pb (351.9 keV), ^{60}Co (1332.5 keV), ^{40}K (1460.8 keV) and ^{208}Tl (2614.6 keV); the detector response proved to be linear over the whole $(0-3)$-MeV range and stable during the measurement campaigns. The four individual calibrated spectra have then been rebinned and merged. The total spectrum is shown in Fig. 4.

From the analysis of the total spectrum, we were able to assess the internal contamination of the Ta sample. Following Ref. [31], we calculated the activities of the various nuclides by reconstructing the detection efficiency of the full-energy peaks (FEPs) with MaGe, a Monte-Carlo simulation code based on the GEANT4 toolkit [32]. The results are listed in Table 3. As it can be seen, the sample is extremely radiopure
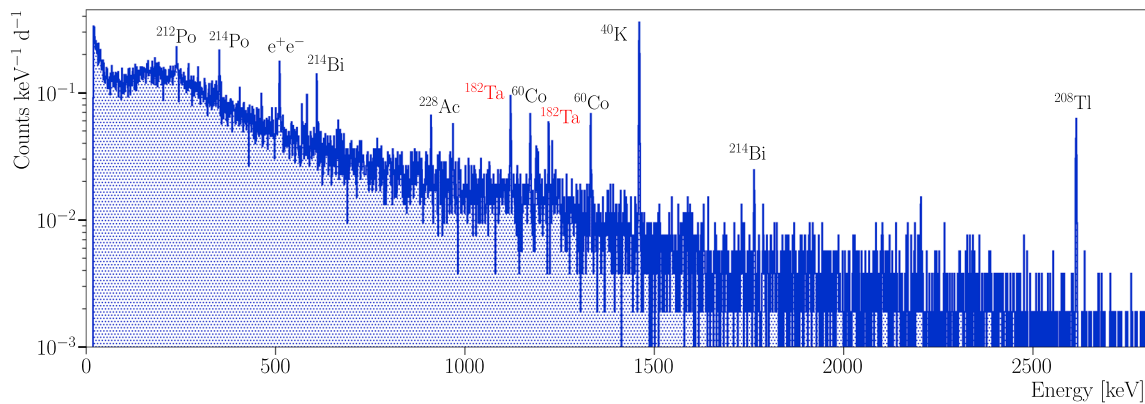
Fig. 4 Sum spectrum of all the acquired runs merged after the calibration of the individual datasets. The total Ta exposure is 2.911 kg year, corresponding to 0.349 g year of ^{180m}Ta

and suitable for rare event searches, showing only ^{40}K and ^{231}Pa concentrations of some hundreds μBq kg^{-1}, the latter value being actually affected by a large uncertainty. In particular, the contribution from ^{182}Ta is subdominant to that of ^{40}K as a result of the 10-year-long storing deep-underground. The ^{182}Ta counting is not compatible with its radioactive decay; the measured 102 μBq kg^{-1} is a weighted average over the whole four-dataset period. This residual activity might be due to a constant activation by the thermal-neutron component at STELLA. Given that the capture cross-section of ^{181}Ta is 20.5 barn [33], this would correspond to a neutron flux of

Table 3 Radionuclide concentrations in the Ta sample measured with an ULB-HPGe detector. For each radionuclide, the activity value is obtained combining the results of the FEPs reported in the table. Measurements are quoted with the related combined expanded uncertainty, while limits are at 90% C.L.

Chain	Nuclide	Peaks (keV)	Activity (μBq kg^{-1})
^{232}Th	^{228}Ra	338.2, 911.2, 969.0	42 ± 10
	^{228}Th	238.6, 583.0, 727.0	55 ± 10
		2614.6	
^{238}U	^{234}Th	92.2, 92.6	< 140
	^{234m}Pa	1001.0	< 650
	^{226}Ra	241.9, 295.2, 351.9	50 ± 5
		609.3, 1120.3, 1764.5	
^{235}U	^{235}U	143.8, 185.7	< 10
	^{231}Pa	300.1, 302.7	680 ± 330
	^{227}Ac	269.5, 271.2	88 ± 33
	^{40}K	1460.8	570 ± 180
	^{137}Cs	661.8	< 5
	^{60}Co	1173.2, 1332.5	< 25
	^{182}Ta	1189.0, 1221.5, 1231.0	102 ± 15^a

^{a}This value is a weighted average of the four datasets

about 7.6×10^{-6} cm^{-2} s^{-1}, a value about an order of magnitude larger than the measured one [15].[2]

The specific analysis of the ^{180m}Ta decay is performed with two fits: the first corresponding to β^- and EC decay channels and the second for the γ de-excitation / IC (Fig. 1). For each branch, we extract a single half-life parameter ($T_{1/2}$) by combining a set of energy windows around the FEP of the γ-ray resulting from the metastable-state decay. In particular, for the β^- mode, we consider one fit region around the FEPs at 234.0 keV, while we do not include the one at 350.9 keV since it almost fully overlaps with a prominent unconstrained FEP of ^{214}Pb at 351.9 keV; we do not include the FEP at 103.6 keV, given the much lower emission probability. This fit window also contains the low energy peak for the or the EC branch, namely the FEP at 215.3 keV. This ensures a common background parametrization for the two peaks of interest, namely 234.0 keV and 215.3 keV. Moreover, for the same fit we define a second window centred at the 332.3 keV line of the EC. We do not include the FEP at 93.3 keV. Finally, for the γ de-excitation/IC mode, we consider a fit with only one region including both FEPs at 93.3 keV and 103.6 keV. The proper de-excitation FEPs of ^{180m}Ta at 37.7 keV and 39.5 keV could not be investigated in this work since the combined detector's encapsulation and sample thickness result in detection efficiencies lower than 10^{-6}.

Each fit window w contains multiple background γ lines at energy E_b and signal γ lines at energy E_s. In general terms, the number of counts at energy E are modeled as:

$$f_w(E) = C_w + D_w E + \sum_b \frac{B_w}{\sqrt{2\pi}\sigma_w} e^{-(E-E_b)^2/2\sigma_w^2}$$
$$+ \sum_s \frac{S_w}{\sqrt{2\pi}\sigma_w} e^{-(E-E_s)^2/2\sigma_w^2} \qquad (1)$$
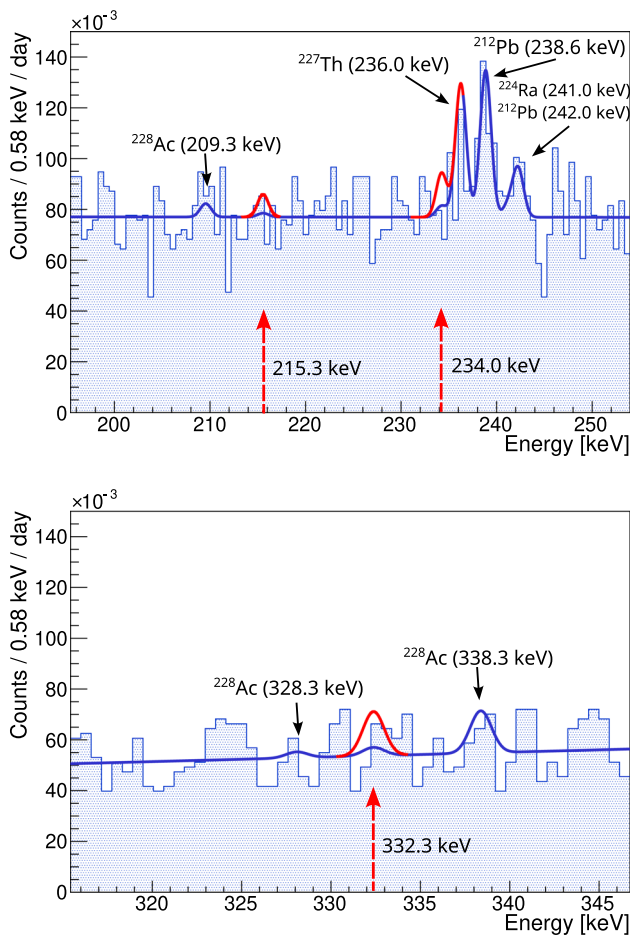

Fig. 5 Fit windows for the β^- and EC decay branches of ^{180m}Ta. The blue lines represent the best fit associated to the posterior mode; the red lines correspond to a signal peak with associated yield from the 90% quantile of the inverse-half-life parameter posterior. The background and signal FEPs are indicated by the solid and dashed arrows, respectively

where C and D are coefficients describing the polynomial component of the background, B and S are the number of counts in the background and signal peaks, while σ is the energy resolution (assumed to be constant inside the window). The signal counts S are connected to the decay half-life through the relation:

$$S(T_{1/2}) = \ln 2 \frac{\epsilon_s \, N_A \, t \, m \, \text{i. a.}}{M} \frac{1}{T_{1/2}}, \qquad (2)$$

where ϵ_s is the detection efficiency of the specific signal γ rays at E_s, N_A is Avogadro's number, t is the measurement live-time ($\sim$ 1.45 year), m is the total sample mass (2015.12 g), M is the molar mass of Ta (180.95) and i. a. is the isotopic abundance of ^{180m}Ta (0.000120).

We perform a Maximum Likelihood fit using the Bayesian Analysis Toolkit (BAT) software package [34]. The likelihood $\mathcal{L}$ is the product over each bin i in each window w of

the Poisson probabilities that contribute to a specific decay branch:

$$\mathcal{L}(\mathbf{p} \mid x) = \prod_w \prod_i \frac{f_{w,i}(\mathbf{p})^{x_i}}{x_i!} e^{-f_{w,i}(\mathbf{p})}, \qquad (3)$$

where $\mathbf{p}$ is the set of free parameters entering the fit and x_i is the number of observed counts in the i-th bin. Referring to Eq. (1), the free parameters in our case are:

– C_w and D_w, set to flat prior probability;
– B_w, set to Gaussian prior if the nuclide activity can be inferred from Table 3, or set to flat probability otherwise;
– σ_w, set to Gaussian prior. Its centroid and width are directly interpolated from the energy-resolution function extracted from dedicated calibration runs[3]
– $T_{1/2}$, set to flat prior probability on the inverse, i. e. on the decay amplitude;
– ϵ_s, set to Gaussian prior probability.

We constrain the fluctuation of the FEP positions by assuming a single energy-scale parameter for both signal and background peaks. For each decay mode, we assign a Gaussian prior to the peak position, centered on the nominal energy and taking its width as the uncertainty from the calibration functions. We assign the same energy-shift parameter to all peaks in the fit window. Finally, we estimate the efficiencies ϵ_s via Monte-Carlo simulations [32] and assume a conservative systematic error of 7%. Uncertainties on the sample mass and isotopic abundance act as scaling parameters in the conversion of the signal strength into a limit on the half-life, however their effect on the final result is negligible. After marginalising the posterior probability distribution for the parameter of interest, i. e. the inverse of $T_{1/2}$, we extract the 0.9 quantile representing the 90% credibility interval (C. I.). This is the value we quote as a limit.

5 Results

The fits of the three decay branches are shown in Figs. 5 and 6, while the details of all the regions of interest (ROIs) are reported in Table 4. The ^{180m}Ta peak counts are consistent with zero counts within 1σ in all cases and no signal has been observed; we therefore quote limits on the half-life of each decay channel.

The first window of the β^- and EC fit (Fig. 5, top) also includes the background FEPs from ^{228}Ac (209.3 keV), ^{227}Th (236.0 keV), ^{212}Pb (238.6 keV), ^{214}Pb (242.0 keV)

---

[3] We interpolated the energy-resolution function with the following polynomial function: $\sigma(E) = 0.504 + 3.4 \times 10^{-4}$; $E - 5.7 \times 10^{-8} E^2$, where the energy E is in keV.
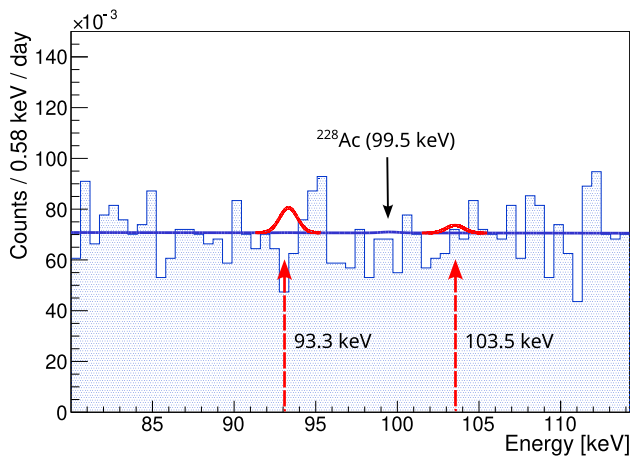
Fig. 6 Fit window for the γ de-excitation/IC decay branch of ^{180m}Ta. The blue line represents the best fit associated to the posterior mode; the red lines correspond to a signal peak with associated yield from the 90% quantile of the inverse-half-life parameter posterior. The background and signal FEPs are indicated by the solid and dashed arrows, respectively

and ^{224}Ra (241.0 keV). The second window (Fig. 5, bottom) contains background peaks from ^{228}Ac (328.0 keV and 338.3 keV). The resulting limits are:

$$T_{1/2,\,\beta^-} > 1.1 \times 10^{18}\text{year (90\% C. I.)} \quad (4)$$

$$T_{1/2,\,\text{EC}} > 1.6 \times 10^{18}\text{year (90\% C. I.)} \quad (5)$$

which corresponds to an improvement by almost a factor 20 for the β^- branch and around one order of magnitude for the EC decay with respect to the current most stringent limits [9,27]. For comparison purposes with other works we also can quote a combined limit by summing the two partial decay constants from which we extract: $T_{1/2,\,\text{EC}+\beta^-} > 6.5 \times 10^{17}$ year (90% C. I.).

Finally, Fig. 6 shows the fit of the γ de-excitation / IC mode. The same ROI includes the two FEPs at 93.3 keV and 103.6 keV, together with an expected background line from ^{228}Ac (99.5 keV). The lower half-life limit is

$$T_{1/2,\,\text{IC}} > 4.1 \times 10^{15}\text{year (90\% C. I.)}, \quad (6)$$

gaining an improvement of a factor 30 with respect to the current bound [28].

6 Constraints on dark matter

The study of ^{180m}Ta is also valuable to constrain specific Dark Matter (DM) scenarios, as outlined in Ref. [35] and demonstrated in Ref. [28]. The general idea is that the nuclear energy stored in the metastable state of an isomer could be released due to DM interactions, so to create an experimental signature or to accelerate the DM particles. ^{180m}Ta is of particular interest due its stability, allowing for experiments in low-background environments to be competitive.

In strongly-interacting DM scenarios, the DM particles can interact with the overburden of an underground laboratory, hence slowing down from their initial galactic velocity distribution. Depending on the magnitude of the DM-nucleon cross-section and on the DM-particle mass, a full thermalization could take place in the overburden and in the end the DM particles might not have sufficient kinetic energy to produce detectable nuclear recoils in large-scale WIMP detectors. In this scenario, the thermalized DM could still interact with the metastable state of ^{180m}Ta, leading to its de-excitation by absorbing the angular momentum of the $9^- \rightarrow 2^+$ transition. The experimental signature is the decay of the ^{180}Ta ground state and it is identical to the γ / IC decay branches investigated in this work; therefore a positive observation of this decay would not be immediately indicative of a DM de-excitation. The smoking-gun for a DM-dominated de-excitation of ^{180m}Ta would be an overburden-dependent half-life of the decay (scaling with the DM density) and would necessitate of multiple measurements in different underground laboratories. However, a non-observation can be used to constrain both the γ / IC decay branch and DM de-excitation simultaneously.

Using the half-life limit for the γ / IC decay branch in Eq. (6) and the same procedure outlined in Ref. [28], we obtain the exclusion plots shown in Fig. 7. In the figure, we represent three DM scenarios, corresponding to as many fractions of the strongly-interacting component over the total
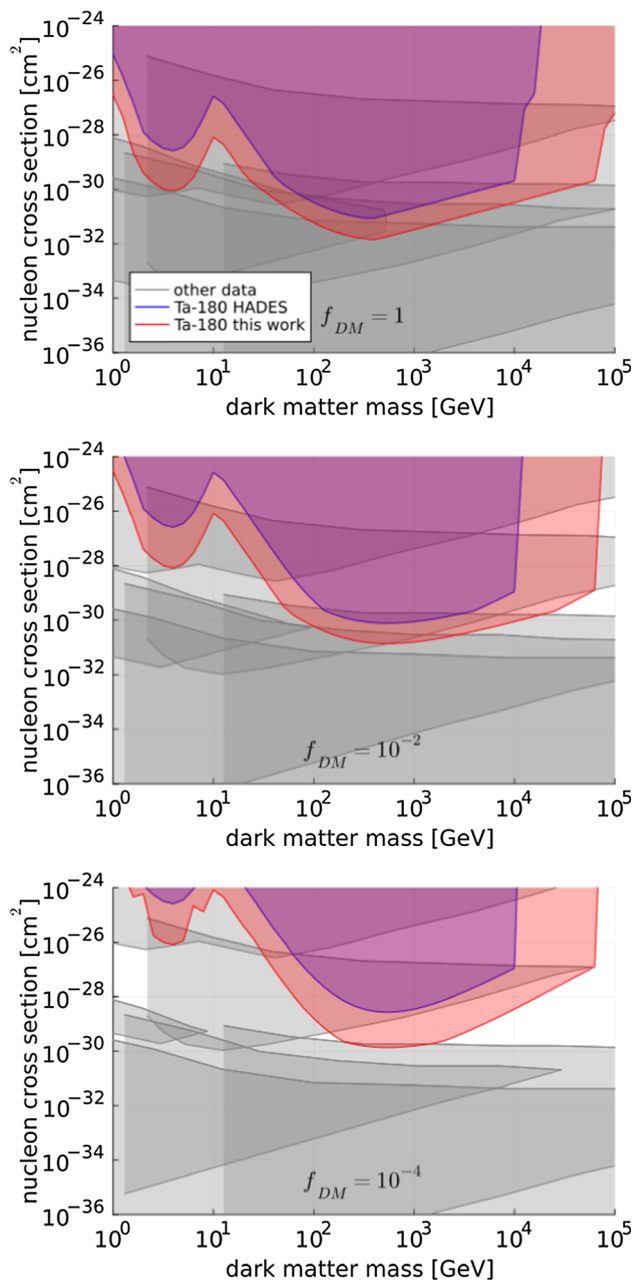
Table 4 Description of the fit windows. For each ROI, the detection efficiency ϵ_s, the FWHM resolution, the background FEPs and the expected contribution B are reported (refer to Eq. (1))

Channel	ROI (keV)	^{180m}Ta FEP (keV)	Efficiency (%)	FWHM (keV)	Bkg FEPs(keV)	Bkg counts (c keV^{-1} kg^{-1} d^{-1})
β^-	195.3–254	234.0	1.56	1.37 ± 0.01	236.0, 238.6, 241.0, 242.0	0.063
EC	195.3–254	215.3	1.30	1.35 ± 0.01	209.3	0.063
	318–347	332.3	2.70	1.44 ± 0.01	328.0, 338.3	0.047
γ/IC	80–115	93.3	0.0036^a	1.26 ± 0.01	99.5	0.06
		103.5	0.0011^a	1.26 ± 0.01	99.5	0.06

^{a}This value also includes the branching ratio

Fig. 7 Exclusion plots for strongly-interacting DM. The three cases represent as many scenarios in terms of fraction of strongly-interacting DM over the total DM density in the Solar System. From top to bottom: 100%, 1% and 0.01%. The gray areas are the regions previously excluded by other experimental searches (see Ref. [28] and references therein). The purple area indicates the region currently excluded by the study of ^{180m}Ta in HADES, while the red area that excluded in this work. The tighter limits on the γ / IC decay branch enhance the probing power to smaller nucleon-DM cross-sections. The greater rock overburden of LNGS extends the exclusion to higher masses. It can be seen that unexplored fractions of the parameter-space have now been probe for scenarios with a fraction of strongly-interacting DM of 1% or less

DM, namely 100%, 1% and 0.01%. The limits coming from other experimental searches are rendered in gray, while the

previous bounds from ^{180m}Ta are shown in purple and the new limits from this work are shown in red. In the case where 100% of the galactic DM density consists of strongly interacting DM (top panel), the parameter-space has already been probed by shallow-depth, surface, or air-borne DM detectors. Here, ^{180m}Ta provides a uniquely different exclusion for this DM scenario. In the scenario where 1% of the galactic DM density consists of strongly interacting DM (central panel), unconstrained regions exist; here we can exclude new parameter space, namely for masses above 10^4 GeV. Finally, for a sub-component fraction of 0.01%, large areas of the parameter-space previously unconstrained, have now been excluded from 10^2 to 10^5 GeV.

The main differences between the previous search with ^{180m}Ta [28] and the current work are, on the one side, the improved half-life limit from 1.3×10^{14} year to 4.1×10^{15} year (90% C.I.); on the other, the increased overburden from 225 m of HADES to 1400 m of LNGS. The former factor enhances the probing power to smaller nucleon-DM cross-sections. The latter extends the exclusion to higher masses, as heavier DM particles are better thermalized in the overburden, thus increasing the DM density inside the detector.

We also considered other composite DM models based on ^{180m}Ta measurements, as described in Ref. [28]. However, these have now been surpassed by measurements in other isotopes [36]: the probed higher DM mass-splittings and the lower cross sections make ^{180m}Ta not competitive anymore.

7 Outlook and perspectives

The new limits on the decay of ^{180m}Ta reported in this paper improve the previous ones by at least one order of magnitude. These results were obtained because of the excellent performance of the ULB-HPGe in the STELLA laboratory, combined with the reduction of the ^{182}Ta background to a subdominant level due to the 10-year-long storage deep-underground.

There are different possible strategies to further improve the experimental sensitivity. The simplest way would be to increase the measurement time. In the current setup, a 5-year-long measurement would translate into a gain of a factor ~ 2. However, in a background-limited detector, the sensitivity scales as $T_{1/2} \propto \varepsilon \cdot B^{-1/2}$ [37], therefore increasing the detection efficiency ε by optimising the sample geometry would be more effective than reducing the background B.

A valid method to enhance the detection efficiency consists in using a HPGe detector array as adopted by the TGV collaboration [38]. There, thin foils of the sample material have been inserted between 16 pairs of large-area HPGe detectors stacked in an array structure (in that case, they have been searching for different modes of double beta decay in

[106]Cd). By exploiting the coincidence between neighbouring face-to-face detectors, this method can lead to a strong background reduction (up to a factor 10) along with an increase of the detection efficiency (by a factor 2). Alternatively, the same idea could be implemented by using rather thick Ta samples sandwiched between pairs face-to-face Ge detectors stacked in multiple towers, as it is being currently done with the MAJORANA Demonstrator, where 17.4 kg of Ta are allocated in between 23 HPGe detectors [39].

A further modification of the stacked detector-array approach would be to use a tower of Ge wafers working as cryogenic calorimeters, similar to the light detectors widely utilized in the CUPID-0 [40] or CUPID-Mo [41] experiments. In this approach, Ta metal foils and Ge wafers (both with optimized thickness) could be stacked minimizing the distance between detectors and sources. The typical energy resolution for cryogenic light detectors is about 100 eV FWHM [42], and could be further pushed down to about 20 eV by exploiting the Neganov–Trofimov–Luke amplification [43]. Such an improved energy resolution would help to minimize background contributions to the region of interest, leading to a factor ~ 5 enhancement in the experimental sensitivity.

Half-lives larger than 10^{21} year could be in principle probed by performing a calorimetric measurement – i.e. with the source embedded in the detector – by including Ta into a compound suitable for the use as a scintillator or as a cryogenic calorimeter. Promising materials are for example $LiTaO_3$, Cs_2TaCl_6 [44] or metallic tantalum itself, being a superconductor [45–48]. This approach would especially benefit searches for low-energy γ's, where the improvement in the detection efficiency would be multiple orders of magnitude.

An entirely different approach are indirect searches for increased concentrations of the daughter isotopes [180]W and [180]Hf in geological tantalum samples [49]. Tantalite and columbite minerals can be more than 10^9 year old, allowing for ample time of daughter accumulation. The sensitivity of these geological searches is difficult to predict, crucially depending on trace impurities of tungsten and hafnium in the minerals as well as on the precision and sensitivity of mass spectrometry.

Despite the non-observation of [180m]Ta decay thus far, a number of techniques now exist to perform these investigations. With adaptation and tuning of the methods described above, the theoretical predictions are within reach. An observation of one or even multiple decay modes of [180m]Ta would not only be intriguing for understanding the nuclear physics of the longest lived nuclear isomer but also opens an avenue for studying certain dark matter scenarios if the decay is observed in multiple underground setups with different overburden.

Data availibility statement This manuscript has no associated data or the data will not be deposited. [Authors' comment: The only data associated with the current analysis is the energy spectrum, which can be requested to the corresponding author.]

References

1. J. Meija et al., Pure Appl. Chem. **88**, 293 (2016). (IUPAC technical report). https://doi.org/10.1515/pac-2015-0503
2. F.A. White, T.L. Collins, F.M. Rourke, Phys. Rev. **97**, 566 (1955). https://doi.org/10.1103/PhysRev.97.566
3. F.A. White, T.L. Collins, F.M. Rourke, Phys. Rev. **101**, 1786 (1956). https://doi.org/10.1103/PhysRev.101.1786
4. J.R. de Laeter, N. Bukilic, Phys. Rev. C **72**, 025801 (2005). https://doi.org/10.1103/PhysRevC.72.025801
5. P. Mohr, F. Kaeppeler, R. Gallino, Phys. Rev. C **75**, 012802 (2007). https://doi.org/10.1103/PhysRevC.75.012802
6. K.L. Malatji et al., Phys. Lett. B **791**, 403 (2019). https://doi.org/10.1016/j.physletb.2019.03.013
7. H. Ejiri, T. Shima, J. Phys. G **44**(6), 065101 (2017). https://doi.org/10.1088/1361-6471/aa65f0
8. W.M. Chan, Study of [180m]Ta decay and development of ultra-low background gamma-ray spectrometry. Ph.D. thesis dissertation. (2017). https://doi.org/10.18910/61506
9. W.M. Chan et al., AIP Conf. Proc. **1921**(1), 030004 (2018). https://doi.org/10.1063/1.5018991
10. C. Arpesella, Appl. Radiat. Isotopes **47**, 991 (1996). https://doi.org/10.1016/S0969-8043(96)00097-8
11. M. Laubenstein, Int. J. Mod. Phys. A **32**(30), 1743002 (2017). https://doi.org/10.1142/S0217751X17430023
12. P.G. Catalano, G. Cavinato, F. Salvini, M. Tozzi, Mem. Soc. Geol. It. **35**, 647 (1986)
13. M. Ambrosio et al., Phys. Rev. D **52**, 3793 (1995). https://doi.org/10.1103/PhysRevD.52.3793
14. G. Bellini et al., JCAP **05**, 015 (2012). https://doi.org/10.1088/1475-7516/2012/05/015
15. A. Best, J. Görres, M. Junker, K.L. Kratz, M. Laubenstein, A. Long, S. Nisi, K. Smith, M. Wiescher, Nucl. Instrum. Methods A **812**, 1 (2016). https://doi.org/10.1016/j.nima.2015.12.034

16. E.A. McCutchan, Nucl. Data Sheets **126**, 151 (2015). https://doi.org/10.1016/j.nds.2015.05.002

17. B. Singh, Nucl. Data Sheets **130**, 21 (2015). https://doi.org/10.1016/j.nds.2015.11.002

18. P. Eberhardt, J. Geiss, C. Lang, W. Herr, E. Merz, Z. Naturforsch. A **10**, 796 (1955). https://doi.org/10.1515/zna-1955-9-1023

19. P. Eberhardt, P. Signer, W. Herr, E. Merz, Z. Naturforsch. A **13**, 1004 (1958). https://doi.org/10.1515/zna-1958-1114

20. E.R. Bauminger, S.G. Cohen, Phys. Rev. **110**, 953 (1958). https://doi.org/10.1103/PhysRev.110.953

21. K. Sakamoto, Nucl. Phys. A **103**(1), 134 (1967). https://doi.org/10.1016/0375-9474(67)90793-2

22. G. Ardisson, Radiochem. Radioanal. Lett. **29**, 7 (1977)

23. E.B. Norman, Phys. Rev. C **24**, 2334 (1981). https://doi.org/10.1103/PhysRevC.24.2334

24. J.B. Cumming, D.E. Alburger, Phys. Rev. **31**, 1494 (1985). https://doi.org/10.1103/PhysRevC.31.1494

25. M. Hult, J. Gasparro, G. Marissens, P. Lindahl, U. Wätjen, P.N. Johnston, C. Wagemans, M. Köhler, Phys. Rev. C **74**, 054311 (2006). https://doi.org/10.1103/PhysRevC.74.054311

26. M. Hult, J.S. Elisabeth Wieslander, G. Marissens, J. Gasparro, U. Wätjen, M. Misiaszek, Appl. Radiat. Isotopes **67**, 918 (2009). https://doi.org/10.1016/j.apradiso.2009.01.057

27. B. Lehnert, M. Hult, G. Lutter, K. Zuber, Phys. Rev. C **95**(4), 044306 (2017). https://doi.org/10.1103/PhysRevC.95.044306

28. B. Lehnert, H. Ramani, M. Hult, G. Lutter, M. Pospelov, S. Rajendran, K. Zuber, Phys. Rev. Lett. **124**(18), 181802 (2020). https://doi.org/10.1103/PhysRevLett.124.181802

29. H. Neder, G. Heusser, M. Laubenstein, Appl. Radiat. Isotopes **53**, 191 (2000). https://doi.org/10.1016/S0969-8043(00)00132-9

30. G. Heusser, M. Laubenstein, H. Neder, Radioact. Environ. **8**, 495 (2006). https://doi.org/10.1016/S1569-4860(05)08039-3

31. M. Heisel, F. Kaether, H. Simgen, Appl. Radiat. Isotopes **67**(5), 741 (2009). https://doi.org/10.1016/j.apradiso.2009.01.028

32. M. Boswell et al., IEEE Trans. Nucl. Sci. **58**(3), 1212 (2011). https://doi.org/10.1109/TNS.2011.2144619

33. S. Nakamura, Y. Shibahara, S. Endo, A. Kimura, J. Nucl. Sci. Technol. **10**, 1061 (2021). https://doi.org/10.1080/00223131.2021.1908187

34. A. Caldwell, D. Kollar, K. Kroninger, Comput. Phys. Commun. **180**, 2197 (2009). https://doi.org/10.1016/j.cpc.2009.06.026

35. M. Pospelov, S. Rajendran, H. Ramani, Phys. Rev. D **101**(5), 055001 (2020). https://doi.org/10.1103/PhysRevD.101.055001

36. N. Song, S.S. Nagorny, A.C. Vincent, Phys. Rev. D **104**, 103032 (2021). https://doi.org/10.1103/PhysRevD.104.103032

37. B. Broerman, M. Laubenstein, S. Nagorny, N. Song, A.C. Vincent, Nucl. Phys. A **1012**, 122212 (2021). https://doi.org/10.1016/j.nuclphysa.2021.122212

38. N.I. Rukhadze et al., Nucl. Phys. A **852**, 197 (2011). https://doi.org/10.1016/j.nuclphysa.2011.01.006

39. Majorana Collaboration, Tantalizing decay of nature's rarest isotope may finally be within reach (2022). https://sanfordlab.org/article/tantalizing-decay-natures-rarest-isotope-may-finally-be-within-reach; https://arxiv.org/abs/2306.01965

40. O. Azzolini et al., Eur. Phys. J. C **78**(5), 428 (2018). https://doi.org/10.1140/epjc/s10052-018-5896-8

41. E. Armengaud et al., Eur. Phys. J. C **80**(1), 44 (2020). https://doi.org/10.1140/epjc/s10052-019-7578-6

42. D.R. Artusa et al., Eur. Phys. J. C **76**(7), 364 (2016). https://doi.org/10.1140/epjc/s10052-016-4223-5

43. L. Bergé et al., Phys. Rev. C **97**(3), 032501 (2018). https://doi.org/10.1103/PhysRevC.97.032501

44. A.M. Tehrani, J. Soh, J. Pásztorová, M.E. Merkel, I. Živković, H.M. Rønnow, N.A. Spaldin, Phys. Rev. Res. **5**(1), L012010 (2023). https://doi.org/10.1103/PhysRevResearch.5.L012010

45. Y. Hochberg, M. Pyle, Y. Zhao, K.M. Zurek, JHEP **08**, 057 (2016). https://doi.org/10.1007/JHEP08(2016)057

46. J. Billard et al., J. Phys. G **44**(10), 105101 (2017). https://doi.org/10.1088/1361-6471/aa83d0

47. L. Pattavina, J.W. Beeman, M. Clemenza, O. Cremonesi, E. Fiorini, L. Pagnanini, S. Pirro, C. Rusconi, K. Schäffner, Eur. Phys. J. A **55**(8), 127 (2019). https://doi.org/10.1140/epja/i2019-12809-0

48. C. Augier et al., J. Low Temp. Phys. **212**, 127 (2023). https://doi.org/10.1007/s10909-023-02971-5

49. L. Bjoern, J. Phys. Conf. Ser. **2156**, 012032 (2021). https://doi.org/10.1088/1742-6596/2156/1/012032